Temporal Scaling of Human Scalp-Recorded Potentials During Interval Estimation

Cameron D. Hassall, Jack Harley, Nils Kolling, and Laurence T. Hunt*

Oxford Centre for Human Brain Activity, Wellcome Centre for Integrative Neuroimaging,

Department of Psychiatry, University of Oxford, Oxford OX3 7JX, United Kingdom

*laurence.hunt@psych.ox.ac.uk

Abstract

Standard event-related potential analysis assumes fixed-latency responses relative to experimental events – yet recent single unit recordings have revealed neural activity *scales* to span different durations during behaviours demanding flexible timing. We use a novel approach to unmix fixed-time and scaled-time components in human electroencephalography, recorded across three tasks. A consistent and distinct scaled-time component is revealed, demonstrating temporal scaling can reliably be measured at the scalp.

Introduction

Action and perception in the real world require flexible timing. We can walk quickly or slowly, recognize the same piece of music played at different tempos, and form temporal expectations over long and short intervals. Flexible timing is critical in our lives, yet its neural correlates have proven difficult to study. One source of difficulty is disagreement over how the brain represents time. For example, the classic pacemaker-accumulator model (Treisman, 1963) relies on a dedicated timing mechanism. Other models represent time intrinsically through oscillatory alignment (Matell & Meck, 2004) or network population dynamics (Buonomano & Maass, 2009). However, it has recently been shown that brain activity at the level of individual neurons can be best explained by a *temporal scaling* mode (Wang et al., 2018).

When monkeys are cued to produce either a short or a long interval, medial frontal cortex (MFC) unit activity can be explained by a single response that is stretched or compressed according to the length of the produced interval – a temporally scaled response. This suggests that flexible motor timing is achieved by adjusting the speed of a common neural process. Temporal scaling of neural responses is also implicit in other settings, such as the process of evidence integration during decision making (O'Connell et al., 2018). Indeed, recent approaches to studying time-warped responses in neural populations have revealed time-warping as a common property across many different population recordings (Williams et al., 2020).

It is currently unclear how temporal scaling of neural responses may manifest at the scalp (if at all) using non-invasive recording in humans. Although electroencephalography (EEG) has played a prominent role in understanding the neural basis of timing (Macar & Vidal, 2004), the method commonly used to analyse such data has been the event-related potential (ERP), which averages event-locked EEG across multiple repetitions. This implicitly assumes

26   that neural activity occurs at *fixed-time* latencies with respect to experimental events.

27   Sometimes these event-related potentials have been found to ramp at different speeds for

28   different temporal intervals (Macar & Vidal, 2004), perhaps suggestive of temporal scaling -

29   but crucially, they appear mixed at the scalp with fixed-time components, due to the

30   *superposition problem* (Chapter 2 in Luck, 2014).

31   We therefore developed an approach to *unmix* scaled-time and fixed-time components in

32   the EEG, which we first tested on simulated data (Fig. 1a). Our proposed method builds on

33   existing regression-based approaches (Ehinger & Dimigen, 2019; Smith & Kutas, 2015a) that

34   have proven useful in unmixing fixed-time components that overlap, e.g. stimulus-related

35   activity and response-related activity. These approaches estimate the ERP using a general

36   linear model (GLM) in which the design matrix is filled with time-lagged dummy variables

37   (1s around the events of interest, 0s otherwise). Importantly, these 'stick functions' can

38   overlap in time to capture overlap in the underlying neural responses (Fig. 1b); in situations

39   without any overlap, the GLM would exactly return the conventional ERP. To reveal scaled-

40   time responses, we allowed the duration of the stick function to vary depending upon the

41   interval between stimulus and response, meaning that the same neural response could span

42   different durations on different trials. As such, the returned scaled-time potential is no longer

43   a function of real-world ('wall clock') time, but instead a function of the *percentage of time*

44   *elapsed* between stimulus and response.

Results

46   As a proof of concept, we simulated data for at a single EEG sensor for an interval timing

47   task, consisting of two *fixed-time components* (locked to cues and responses), and one *scaled-*

4
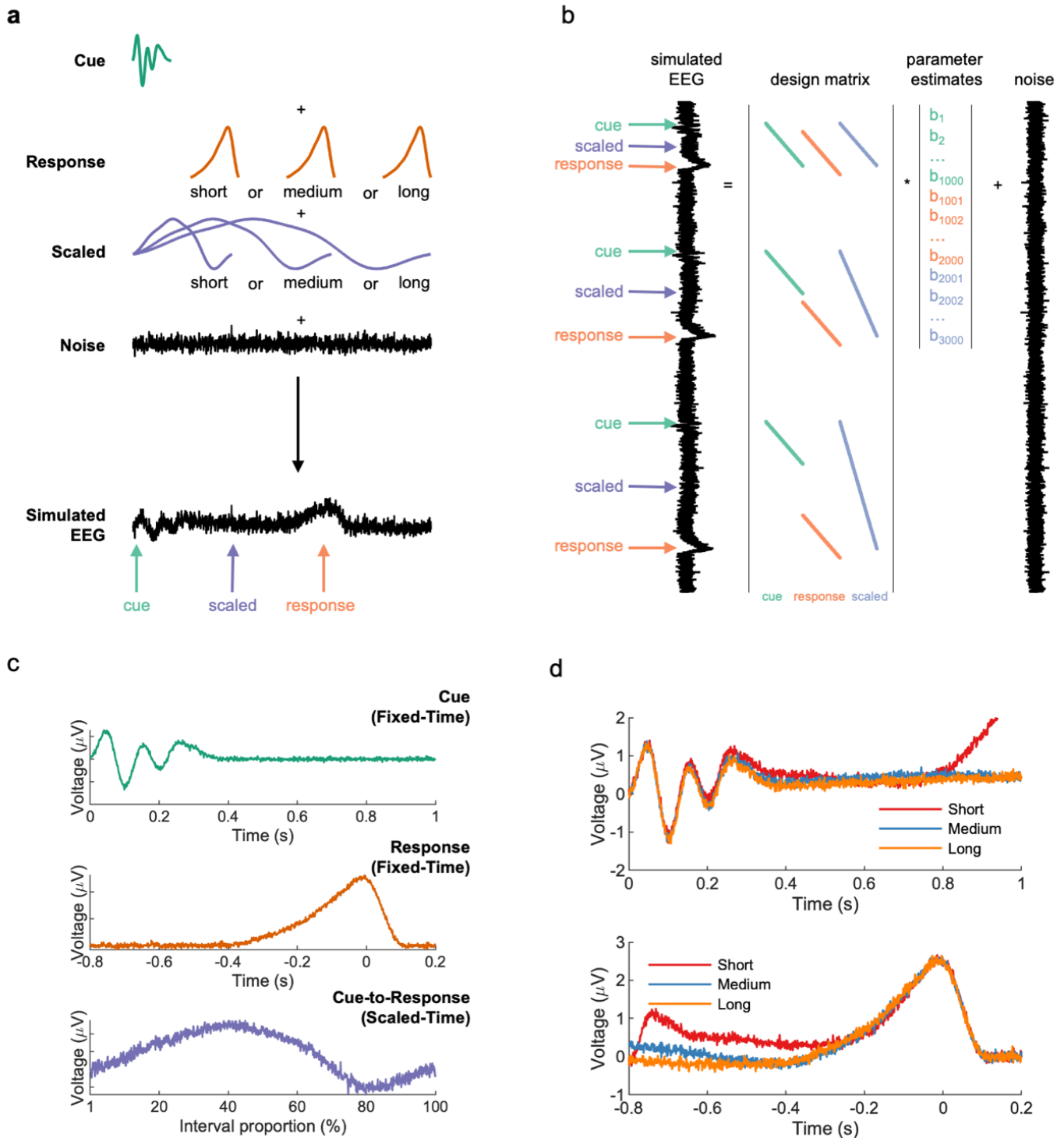
Figure 1. **Regression based unmixing of simulated data successfully recovers scaled-time and fixed-time components.** (a) EEG data were simulated by summing fixed-time components (cue and response), a scaled-time component with differing durations for different trials (short, medium, or long), and noise. (b) The simulated responses were unmixed via a GLM with stick basis functions: cue-locked, response-locked, and a single scaled-time basis spanning from cue to response. (c) The GLM successfully recovered all three components, including the scaled-time component. (d) A conventional ERP analysis (cue-locked and response-locked averages) of the same data obscured the scaled-time component.

48   *time component* spanning between cues and responses (Fig. 1a). Our proposed method was

49   successful in recovering all three components (Fig. 1c), whereas a conventional ERP

5

50   approach obscured the scaled-time component (Fig. 1d). Crucially, in real EEG data we also

51   repeat this approach across all sensors, potentially revealing different scalp topographies (and

52   hence different neural sources) for fixed-time versus scaled-time components.

53   We used this approach to analyze EEG recorded during three interval timing tasks

54   (Supplementary Fig. 1). In one task, participants produced a target interval (short, medium, or

55   long) following a cue. Feedback was provided, and participants were able to closely match

56   the target intervals. In a second, participants evaluated a computer-produced interval. The

57   closer the produced interval was to the target interval, the more likely participants were to

58   judge the response as 'on time'. In a third (previously analyzed (Breska & Deouell, 2017a,

59   2017b)) task, participants made temporal predictions about upcoming events based on

60   rhythmic predictions.

61   In all three tasks, we observed a scaled-time component that was distinct from the

62   preceding and following fixed-time components (Fig. 2), which resembled conventional

63   ERPs (Supplementary Fig. 3). Typically, ERP components are defined by their polarity, scalp

64   distribution, and latency (Luck, 2014). The observed scaled-time components shared a

65   common polarity (negative) and scalp distribution (central), which is notably consistent with

66   the medial frontal recording site where temporally scaled single-unit responses were

67   previously identified (Wang et al., 2018). Although our scaled-time components were

68   estimated by time-warping a common signal so that they could span a variable delay period,

69   their 'latency' was nevertheless consistent, in that the scaled-time signal grew and appeared

70   to peak later in the timed interval. This is again reminiscent of the time course of scaled time
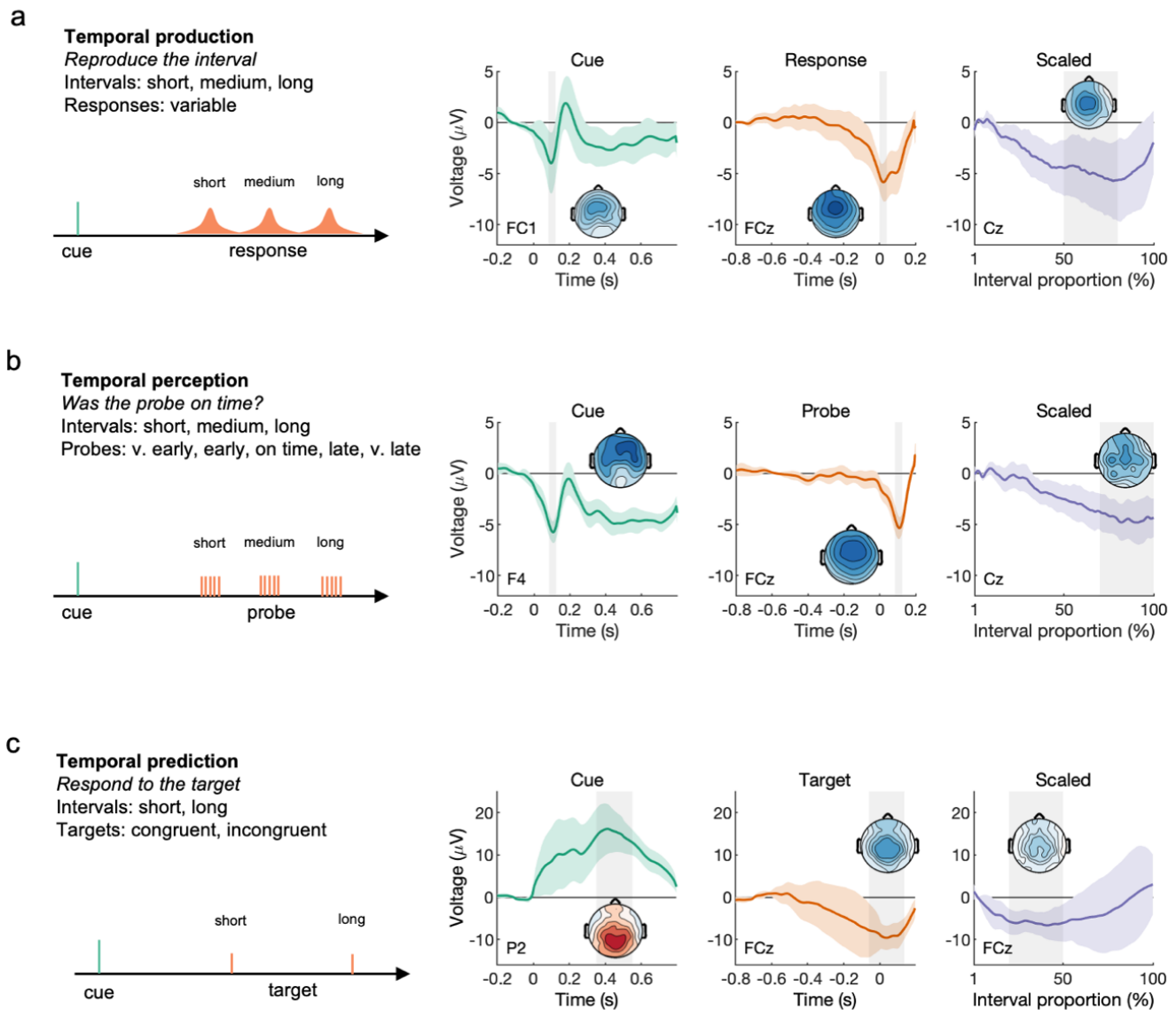
Figure 2. **Scaled-time components were consistently observed across three time-estimation paradigms, with distinct scalp topographies from fixed-time components.** Data were analysed from: (a) a temporal production task; (b) a temporal judgement task; (c) a temporal prediction task[11,12]. All had distinct fixed-time components relative to task-relevant events (left/middle columns), and a common negative scaled-time component over central electrodes, reflecting interval time (right column). Error bars represent 95% confidence intervals.

71   components across the neural population in medial frontal recordings (Wang et al., 2018).

72   Single-sample *t*-tests of the mean voltage in the shaded regions in Fig. 2 revealed a

73   significant scaled-time signal in the production task ($t(9)$ = -3.19, p = .01, Cohen's d = -

74   1.01), the perception task ($t(9)$ = -4.79, p = .001, Cohen's d = -1.52), and the prediction task

75   ($t(18)$ = -4.03, p < .001, Cohen's d = -0.92). In many cases, scaled-time components were

76   reliably observed at the single-subject level (Supplementary Figs. 4-6).

77   We then examined how the scaled-time component related to behavioural variability:

78   does the latency of the scaled-time component predict participants' response time? To

79   measure component latency, we applied an approach developed in Hunt et al. (2015) and

80   Möcks (1986), using principal component analysis (PCA) to model delay activity over central

81   electrodes in the temporal production task, after first regressing out fixed-time components

82   from the data. PCA was applied separately to each of three produced intervals. This

83   consistently revealed a first principal component that matched the shape of the scaled-time

84   component identified in Fig. 2a, and a second principal component that matched its *temporal*

85   *derivative*. This analysis not only provides an additional way of confirming the presence of

86   the scaled-time component in our data (as it is the first principal component of the residuals

87   after removing fixed-time components), but crucially adding or subtracting PC2 captures

88   variation in the *latency* of this scaled-time component (Fig. 2b). Across response time

89   quantiles, we found that PC2 scores were significantly related to response times (Fig. 3c;

90    $F(2,18) = 9.05$, $p = .002$). This implies that the earlier in time that the scaled-time component

91   peaked, the faster the subject would respond on that trial. Note, however, that within-

92   condition behaviour was highly consistent in Task 1 (Supplementary Fig. 2); we would

93   therefore expect the relationship between scaled-time component latency and behaviour to be

94   even stronger in tasks with greater response variability between trials.
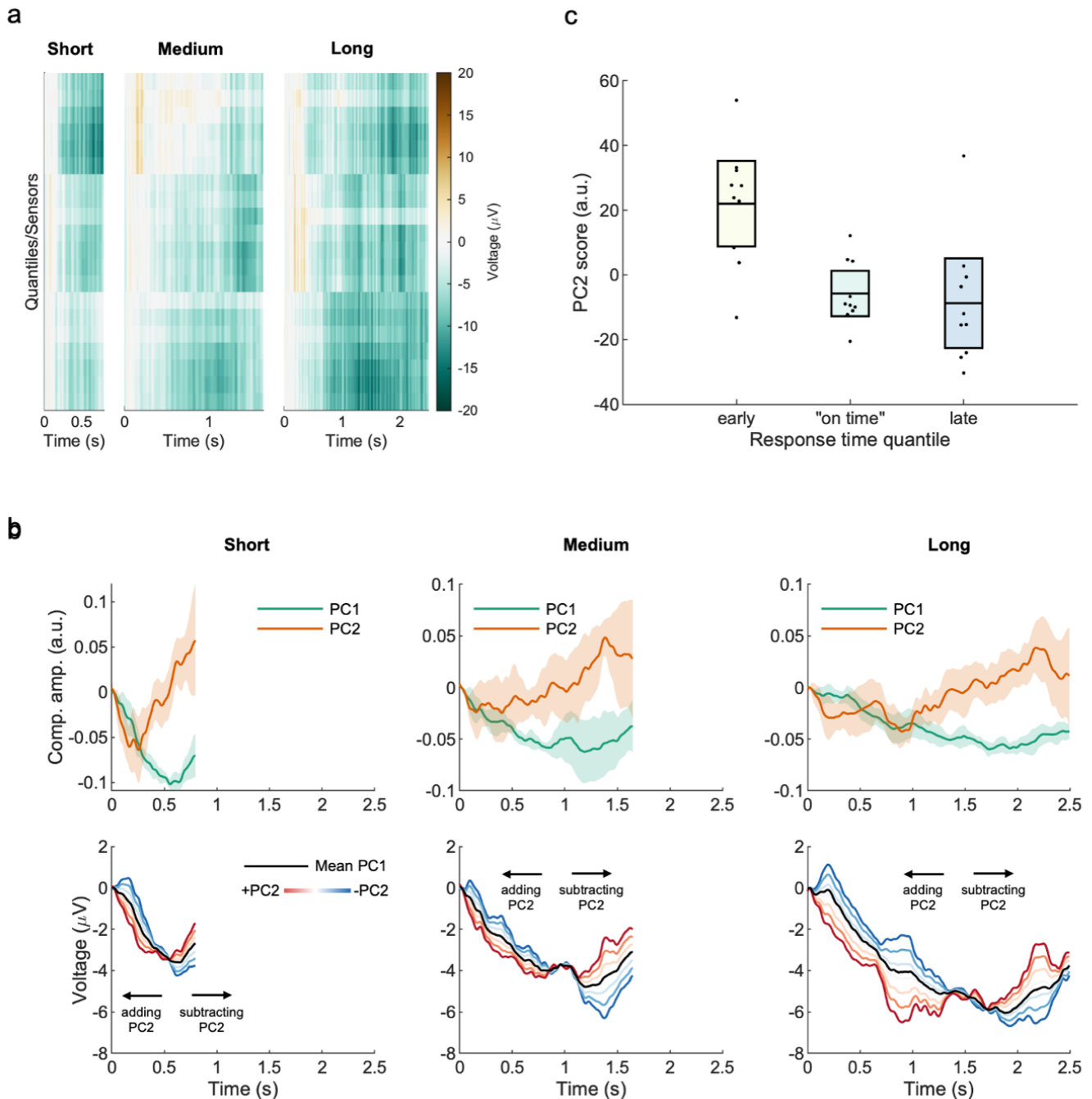
Figure 3. **Variation in scaled-time components predict behavioural variation in time estimation.** (a) Cue-locked EEG over central electrodes (FC1, FCz, FC2, Cz, CP1, CPz, CP2) was grouped by response time (early, on time, or late), averaged, and stacked for each target interval (short, medium, or long). Data for one participant is shown. A separate PCA was run for each target interval and participant. (b) The first two principal components for each target interval represent the amplitude (PC1) and first derivative (PC2) of the time-scaled component (top panel). Adding or subtracting different amounts of PC2 to PC1 shifted the peak earlier or later in time (bottom panel). (c) PC2 scores depended on response time, implying the scaled-time component peaked earlier for fast responses and later for slow responses. Error bars represent 95% confidence intervals.

Discussion

95   Our results provide a general method for recovering temporally scaled signals in

96   human EEG, where scaled-time components are mixed at the scalp with conventional fixed-

98 time ERPs. We focused here on interval production and perception, but we anticipate other

99 temporally scaled EEG and MEG signals will be discovered for cognitive processes known to

100 unfold over varying timescales. For example, the neural basis of flexible sequential

101 behaviours (such as speech) is still unknown, but may involve a form of temporal scaling

102 (Remington et al., 2018). Flexible timing is also important in decision-making tasks, where

103 evidence accumulation can proceed quickly or slowly depending on the strength of the

104 evidence (O'Connell et al., 2018). Flexible timing can help facilitate a range of adaptive

105 behaviours via *temporal attention* (Nobre & van Ede, 2018), while disordered timing

106 characterizes several clinical disorders (Allman & Meck, 2012), underscoring the importance

107 of characterising temporal scaling of neural responses in human participants.

Acknowledgements

Author Contributions

N.K. and L.T.H. conceived the experiments and methodology. C.D.H. and L.T.H. designed the experiments and developed the methodology. C.D.H. and J.H. performed the experiments (except for the prediction task, where data was downloaded from a previous publication (Breska & Deouell, 2017a, 2017b)). C.D.H. and L.T.H. analyzed the data. C.D.H. and L.T.H. wrote the manuscript with input from the other authors.

Competing interests

The authors declare no competing interests.

Additional information

Supplementary information is available for this paper.

Correspondence and requests for materials should be addressed to L.T.H.

Methods

Simulations

108

109

110   We simulated cue-related and response-related EEG in a temporal production task

111 using MATLAB 2020a (Mathworks, Natick, USA). Cue and response were separated by

112 either a short, medium, or long interval. During the delay period, we simulated a scaled

113 response that stretched or compressed to fill the interval. All three responses (cue, response,

114 scaled) were summed together at appropriate lags (short, medium, or long), with noise – see

115 Fig. 1a. In total, we simulated 50 trials of each condition (short, medium, long).

116   To unmix fixed-time and scaled-time components, we used a regression-based

117 approach (Ehinger & Dimigen, 2019; Smith & Kutas, 2015a, 2015b) in which the continuous

118 EEG at one sensor Y is modelled as a linear combination of the underlying event-related

119 responses β, which are unknown initially. The model can be written in equation form as:

120 $$Y = X\beta + \varepsilon$$

121 where X is the design matrix and ε is the residual EEG not accounted for by the model. X

122 contains as many rows as EEG data points, and as many columns as predictors (that is, the

123 number of points in the estimated event-related responses). In our case, X was populated by

124 'stick functions' – non-zero values around the time of the modelled events, and zeros

125 otherwise. We included in X two fixed-time components, the cue and the response, as stick

126 functions of set EEG duration (with variables set to 1). In other words, the height of the

127 fixed-time stick function was constant across events of the same type and equal to its width.

128 To model a temporally-scaled response, we used the MATLAB *imresize* function (Image

129 Processing Toolbox, R2020b) with 'box' interpolation to stretch/compress a stick function so

130 that it spanned the duration between cue and response (other interpolation methods were tried

131 – see Supplementary Fig. 7 – but this choice had little effect on the results). Thus, the

132 duration of the scaled stick function varied from trial to trial (Fig. 1b). The goal here was to

133   estimate a single scaled-time response to account for EEG activity across multiple varying

134   delay periods. For the fixed-time responses, each column of X represents a latency in ms

135   before/after an experimental event; by contrast, for the scaled-time responses, each column of

136   X represents the *percentage* of time that has elapsed between *two* events (stimulus and

137   response). Simulation code is available at https://git.fmrib.ox.ac.uk/chassall/temporal-scaling.

Production and Perception Tasks

Participants

140   Participants completed both the production and perception tasks within the same

141   recording session. We tested ten university-aged participants, 5 male, 2 left-handed, M_{age} =

142   23.40, 95% CI [21.29, 25.51]. Participants had normal or corrected-to-normal vision and no

143   known neurological impairments. Participants provided informed consent approved by the

144   Medical Sciences Interdivisional Research Ethics Committee at the University of Oxford.

145   Following the experiment, participants were compensated £20 (£10 per hour of participation)

146   plus a mean performance bonus of £3.23, 95% CI [2.92, 3.55].

Apparatus and Procedure

148   Participants were seated approximately 64 cm from a 27-inch LCD display (144 Hz, 1

149   ms response rate, 1920 by 1080 pixels, Acer XB270H, New Taipei City, Taiwan). Visual

150   stimuli were presented using the Psychophysics Toolbox Extension (Brainard, 1997; Pelli,

151   1997) for MATLAB 2014b (Mathworks, Natick, USA). Participants were given written and

152   verbal instructions to minimize head and eye movements. The goal of the production task

153   was to produce a target interval and the goal of the perception task was to judge whether or

154   not a computer-produced interval was correct.

155   The experiment was blocked with ten trials per block. There were 18 production

156   blocks and 18 perception blocks, completed in random order. Prior to each block, participants

157   listened to five isochronic tones indicating the target interval. Beeps were 400 Hz sine waves

158 of duration 50 ms and an onset/offset ramping to a point 1/8 of the length of the wave (to

159 avoid abrupt transitions). The target interval was either short (0.8 s), medium (1.65 s), or

160 long (2.5 s).

161   In production trials, participants listened to a beep then waited the target time before

162 responding. Feedback appeared after a 400-600 ms delay (uniform distribution) and remained

163 on the display for 1000 ms. Feedback was a 'quarter-to' clockface to indicate 'too early', a

164 'quarter-after' clockface to indicate 'too late', or a checkmark to indicate an on-time

165 response. Feedback itself was determined by where the participant's response fell relative to a

166 window around the target duration. The response window was initialized to +/- 100 ms

167 around each target, then changed following each feedback via a staircase procedure:

168 increased on each side by 10 ms following a correct response and decreased by 10 ms

169 following an incorrect response (either too early or too late).

170   In perception trials, participants heard two beeps, then were asked to judge the

171 correctness of the interval, that is, whether or not the test interval matched the target interval.

172 Test intervals (very early, early, on time, late, very late) were set such that each subsequent

173 interval was 25% longer than the previous (see Supplementary Table 1). Participants were

174 then given feedback on their judgement – a checkmark for a correct judgement, or an 'x' for

175 an incorrect judgement.

176   For each task, participants gained 2 points for each correct response and lost 1 point

177 for each incorrect response. At the end of the experiment points were converted to a monetary

178 bonus at a rate of £0.01 per point.

179 ***Data Collection***

180   In the perception task we recorded participant response time from cue, trial outcome

181 (early, late, on time), and staircase- response window. In the production task, we recorded

182 trial 'on time' judgements (yes/no), and trial outcome (correct/incorrect).

14

183   We recorded 36 channels of EEG, referenced to AFz. Data were recorded at 1000 Hz

184   using a Synamps amplifier and CURRY 8 software (Compumetrics Neuroscan, Charlotte,

185   USA). The electrodes were sintered Ag/AgCl (EasyCap, Herrsching, Germany). 31 of the

186   electrodes were laid out according to the 10-20 system. Additional electrodes were placed on

187   the left and right mastoids, on the outer canthi of the left and right eyes, and below the right

188   eye. The reference electrode was placed at location AFz, and the ground electrode at Fpz.

189   **Prediction Task**

190   In this previously published (Breska & Deouell, 2017a, 2017b) experiment, 19

191   participants responded to the onset of a visual target following a visual warning cue. The

192   delay between cue and target was either short (700 ms) or long (1300 ms) and, in some

193   conditions, congruent with a preceding stimulus stream. Only these predictable trials were

194   included in the current analysis (i.e., the 'valid' trials in the 'Rhythmic' and 'Repeated-

195   Interval' conditions – see Breska and Deouell, 2017a, 2017b for more detail).

196   **Data Analysis**

197   ***Behavioural data***

198   For the perception task, we computed mean window size and mean produced interval

199   for each participant. For the production task, we computed mean likelihood of responding yes

200   to the 'on time' prompt, for each condition (short, medium, long) and interval (very early,

201   early, on time, late, very late).

202   ***EEG Preprocessing***

203   For all three tasks, EEG was preprocessed in MATLAB 2020b (Mathworks, Natick,

204   USA) using EEGLAB (Delorme & Makeig, 2004). We first down-sampled the EEG to 200

205   Hz, then applied a 0.1-20 Hz bandpass filter and 50 Hz notch filter. The EEG was then re-

206   referenced to the average of the left and right mastoids (and AFz recovered in the

207   production/perception tasks). Ocular artifacts were removed using independent component

208   analysis (ICA). The ICA was trained on 3-second epochs of data following the appearance of

209   the fixation cross at the beginning of each trial. Ocular components were identified using the

210   *iclabel* function and then removed from the continuous data.

211   ***ERPs***

212   To construct conventional event-related potentials (ERPs), we first created epochs of

213   EEG around cues (all tasks), responses (perception task), probes (production task), and

214   targets (prediction task). Cue-locked ERPs extended from 200 ms pre-cue to either 800, 1650,

215   or 2500 ms post-cue (the short, medium, and long targets) in the perception/production tasks

216   and 700 or 1300 ms in the prediction task (the short and long targets). Epochs were baseline-

217   corrected using a 200 ms pre-cue window. We also constructed epochs from 800, 1650, or

218   2500 ms prior to the response/probe in the production/perception tasks and 700 or 1300 ms

219   prior to the target in the prediction task to 200 ms after the response/probe/target. A baseline

220   was defined around the event of interest (mean EEG from -20 to 20 ms) and removed. We

221   then removed any trials in which the sample-to-sample voltage differed by more than 50 μV

222   or the voltage change across the entire epoch exceeded 150 μV. Cue and

223   response/probe/target epochs were then averaged for each participant, task (production,

224   perception, prediction), and condition (short, medium, long). Finally, participant averages

225   were combined into grand-average waveforms at electrode FCz, a location where timing-

226   related activity has been previously observed (Macar & Vidal, 2004). See Supplementary Fig.

227   3.

228   ***rERPs***

229   To unmix fixed-time and scaled-time components in our EEG data, we estimated

230   regression-ERPs (rERPs) following the same GLM procedure we used with our simulated

231   data, but now applied to each sensor. We used a design matrix consisting of a regular stick

232   functions for cue and response/probe/target and a stretched/compressed stick function

16

233   spanning the interval from cue to response/probe/target. In particular, we estimated cue-

234   locked responses that spanned from 200 ms pre-cue to 800 ms post-cue. The

235   response/probe/target response interval spanned from -800 to 200 ms. Each fixed-time

236   response thus spanned 1000 ms, or 200 EEG sample points. The scaled-time component, as

237   described earlier, was modelled as a single underlying component (set width in X) that

238   spanned over multiple EEG durations (varying number of rows in X). Thus, our method

239   required choosing how many scaled-time sample points to estimate (the width in X). For the

240   production/perception tasks, we chose to estimate 330 scaled-time points, equivalent to the

241   duration of the 'medium' interval. For the prediction task, we chose to estimate 200 scaled-

242   time points, equivalent to the mean of the short and long conditions (700 ms, 1300 ms).

243   Unlike the conventional ERP approach, this analysis was conducted on the continuous EEG.

244   To identify artifacts in the continuous EEG, we used the *basicrap* function from the ERPLAB

245   (Lopez-Calderon & Luck, 2014) toolbox with a 150 µV threshold (2000 ms window, 1000

246   ms step size). A sample was flagged if it was 'bad' for any channel. Flagged samples were

247   excluded from the GLM (samples removed from the EEG and rows removed from the design

248   matrix). Additionally, we removed samples/rows associated with unusually fast or slow

249   responses in the production task (less than 0.2 s or more than 5 s). On average, we removed

250   2.17 % of samples in the production task (95% CI [1.49, 2.86]), 3.75 % of samples in the

251   perception task (95% CI [2.39, 5.10]), and 1.03% of samples in the prediction task (95% CI

252   [0.95, 1.10]).

253   To impose a smoothness constraint on our estimates, we used a first-derivative form

254   of Tikhonov regularization. Tikhonov regularization reframes the GLM solution as the

255   minimization of:

256                                    $$\|X\beta - Y\|^2 + \lambda\|L\beta\|^2$$

257   where L is the regularization operator and λ is the regularization parameter. In other words,

258   we aimed to minimize a penalty term in addition to the usual residual. This has the solution

259 $$(X^T X + \lambda L)^{-1} X^T Y$$

260   In our case, L approximated the first derivative as a scaled finite difference (Reichel & Ye,

261   2008):

262 $$L = \frac{1}{2} \begin{bmatrix} 1 & -1 & 0 & ... & 0 & 0 \\ 0 & 1 & -1 & ... & 0 & 0 \\ ... & ... & ... & ... & ... & ... \\ 0 & 0 & 0 & ... & 1 & -1 \end{bmatrix}$$

263   We then chose regularization parameters for each participant using 10-fold cross validation.

264   Our goal here was to minimize the mean-squared error of the residual EEG at electrode FCz,

265   our electrode of interest. The following λs were tested on each fold: 0.001, 0.01, 0, 1, 10,

266   100, 1000, 10000, 100000. An optimal λ was chosen for each participant corresponding to

267   the parameter with the lowest mean mean-squared error across all folds. See Supplementary

268   Table 3 for a summary.

269   ***Inferential Statistics***

270   We quantified the amplitude of the scaled-time component in two ways. First, we

271   computed a 95% confidence interval at each 'timepoint' in the scaled-time signal. Next, in

272   line with conventional ERP analyses (Luck, 2014), we computed the mean signal around the

273   apparent peak. We then confirmed the existence of the signal using a single-sample repeated-

274   measures *t*-test. These analyses were done at the scalp location where the mean signal was

275   greatest, i.e. electrode Cz in the production/perception tasks and FCz in the prediction task.

276   ***PCA***

277   To explore the link between the scaled-time component and behaviour, we regressed

278   out the fixed-time components from the EEG in the temporal production task – that is, we

279   reconstructed the preprocessed data using only the scaled-time regressors plus residuals. Only

280   mid-frontal electrodes were considered: FC1, FCz, FC2, Cz, CP1, CPz, and CP2. We then

281 constructed epochs starting at the cue and ending at the target interval (800 ms, 1650 ms, or

282 2500 ms). Epochs within each condition (short, medium, long) were further grouped into

283 three equal-sized response-time bins (early, on time, late) and averaged for each electrode

284 and participant (Fig. 3a). We then conducted a PCA for each condition (short, medium, long)

285 and participant. See Supplementary Table 2 for amount of variance explained by PC1 and

286 PC2. To visualize the effect of PC2, we computed the mean PC2 across all participants. We

287 then added more or less of the mean PC2 to the mean PC1 projection and applied a 25-point

288 moving-mean window for visualization purposes (Fig. 3b). In order to choose a reasonable

289 range of PC2 scores, we examined the average minimum and maximum PC2 score for each

290 participant and condition (short, medium, long). The PC2 score ranges were -21 to 15 (short),

291 -41 to 38 (medium), and -40 to 55 (long). To assess the relationship between PC2 score and

292 behaviour, we binned PC2 scores according to our response time bins (early, on time, late)

293 and collapsed across conditions (short, medium, long). This gave us as single mean PC2

294 score for each participant and response time bin (early, on time, late), which we analyzed

295 using a repeated-measures ANOVA (Fig. 3c).

296 **Data Availability**

297 Raw and preprocessed EEG for the production and perception tasks will be made publicly

298 available at the time of publication. Raw data for the prediction task is available at

299 https://doi.org/10.5061/dryad.5vb8h.

300 **Code Availability**

301 Simulation and analysis scripts are available at https://git.fmrib.ox.ac.uk/chassall/temporal-

302 scaling.

References

Allman, M. J., & Meck, W. H. (2012). Pathophysiological distortions in time perception and timed performance. *Brain*, *135*(3), 656–677. https://doi.org/10.1093/brain/awr210

Brainard, D. H. (1997). The psychophysics toolbox. *Spatial Vision*, *10*, 433–436.

Breska, A., & Deouell, L. Y. (2017a). *Data from: Neural mechanisms of rhythm-based temporal prediction: delta phase-locking reflects temporal predictability but not rhythmic entrainment* (Version 1, p. 19333644881 bytes) [Data set]. Dryad. http://datadryad.org/stash/dataset/doi:10.5061/dryad.5vb8h

Breska, A., & Deouell, L. Y. (2017b). Neural mechanisms of rhythm-based temporal prediction: Delta phase-locking reflects temporal predictability but not rhythmic entrainment. *PLOS Biology*, *15*(2), e2001665. https://doi.org/10.1371/journal.pbio.2001665

Buonomano, D. V., & Maass, W. (2009). State-dependent computations: Spatiotemporal processing in cortical networks. *Nature Reviews. Neuroscience*, *10*(2), 113–125. https://doi.org/10.1038/nrn2558

Delorme, A., & Makeig, S. (2004). EEGLAB: An open source toolbox for analysis of single-trial EEG dynamics including independent component analysis. *Journal of Neuroscience Methods*, *134*(1), 9–21. https://doi.org/10/bqr2f2

Ehinger, B. V., & Dimigen, O. (2019). Unfold: An integrated toolbox for overlap correction, non-linear modeling, and regression-based EEG analysis. *PeerJ*, *7*, e7838. https://doi.org/10.7717/peerj.7838

Hunt, L. T., Behrens, T. E., Hosokawa, T., Wallis, J. D., & Kennerley, S. W. (2015). Capturing the temporal evolution of choice across prefrontal cortex. *ELife*, *4*, e11945. https://doi.org/10.7554/eLife.11945

Lopez-Calderon, J., & Luck, S. J. (2014). ERPLAB: An open-source toolbox for the analysis of event-related potentials. *Frontiers in Human Neuroscience*, *8*. https://doi.org/10.3389/fnhum.2014.00213

Luck, S. J. (2014). *An introduction to the event-related potential technique* (Second edition). The MIT Press.

Macar, F., & Vidal, F. (2004). Event-Related Potentials as Indices of Time Processing: A Review. *Journal of Psychophysiology*, *18*(2/3), 89–104. https://doi.org/10.1027/0269-8803.18.23.89

Matell, M. S., & Meck, W. H. (2004). Cortico-striatal circuits and interval timing: Coincidence detection of oscillatory processes. *Cognitive Brain Research*, *21*(2), 139–170. https://doi.org/10.1016/j.cogbrainres.2004.06.012

Möcks, J. (1986). The Influence of Latency Jitter in Principal Component Analysis of Event-Related Potentials. *Psychophysiology*, *23*(4), 480–484. https://doi.org/10.1111/j.1469-8986.1986.tb00659.x

Nobre, A. C., & van Ede, F. (2018). Anticipated moments: Temporal structure in attention. *Nature Reviews Neuroscience*, *19*(1), 34–48. https://doi.org/10.1038/nrn.2017.141

O'Connell, R. G., Shadlen, M. N., Wong-Lin, K., & Kelly, S. P. (2018). Bridging Neural and Computational Viewpoints on Perceptual Decision-Making. *Trends in Neurosciences*, *41*(11), 838–852. https://doi.org/10.1016/j.tins.2018.06.005

Pelli, D. G. (1997). The VideoToolbox software for visual psychophysics: Transforming numbers into movies. *Spatial Vision*, *10*(4), 437–442. https://doi.org/10.1163/156856897X00366

Reichel, L., & Ye, Q. (2008). Simple Square Smoothing Regularization Operators. *Electronic Transactions on Numerical Analysis*, *33*, 63–83.

Remington, E. D., Narain, D., Hosseini, E. A., & Jazayeri, M. (2018). Flexible Sensorimotor Computations through Rapid Reconfiguration of Cortical Dynamics. *Neuron*, *98*(5), 1005-1019.e5. https://doi.org/10.1016/j.neuron.2018.05.020

Smith, N. J., & Kutas, M. (2015a). Regression-based estimation of ERP waveforms: I. The rERP framework. *Psychophysiology*, *52*(2), 157–168. https://doi.org/10.1111/psyp.12317

Smith, N. J., & Kutas, M. (2015b). Regression-based estimation of ERP waveforms: II. Nonlinear effects, overlap correction, and practical considerations. *Psychophysiology*, *52*(2), 169–181. https://doi.org/10.1111/psyp.12320

Treisman, M. (1963). Temporal discrimination and the indifference interval: Implications for a model of the 'internal clock'. *Psychological Monographs: General and Applied*, *77*(13), 1–31. https://doi.org/10.1037/h0093864

Wang, J., Narain, D., Hosseini, E. A., & Jazayeri, M. (2018). Flexible timing by temporal scaling of cortical responses. *Nature Neuroscience*, *21*(1), 102–110. https://doi.org/10.1038/s41593-017-0028-6

Williams, A. H., Poole, B., Maheswaranathan, N., Dhawale, A. K., Fisher, T., Wilson, C. D., Brann, D. H., Trautmann, E. M., Ryu, S., Shusterman, R., Rinberg, D., Ölveczky, B. P., Shenoy, K. V., & Ganguli, S. (2020). Discovering Precise Temporal Patterns in Large-Scale Neural Recordings through Robust and Interpretable Time Warping. *Neuron*, *105*(2), 246-259.e8. https://doi.org/10.1016/j.neuron.2019.10.020